Absorption of diffusive spin current in surface and bulk states of a topological insulator

Akiyo Nomura, Nariaki Nasaka, Takaharu Tashiro, Takao Sasagawa, and Kazuya Ando

Phys. Rev. B **96**, 214440 — Published 28 December 2017

DOI: 10.1103/PhysRevB.96.214440

Absorption of diffusive spin current in surface and bulk states of topological insulator

Akiyo Nomura,[1] Nariaki Nasaka,[2] Takaharu Tashiro,[1] Takao Sasagawa,[2] and Kazuya Ando[1,3,*]

[1]*Department of Applied Physics and Physico-Informatics, Keio University, Yokohama 223-8522, Japan*

[2]*Laboratory for Materials and Structures Laboratory, Tokyo Institute of Technology, Kanagawa 226-8503, Japan*

[3]*PRESTO, Japan Science and Technology Agency, Kawaguchi, Saitama 332-0012, Japan*

(Dated: November 20, 2017)

Abstract

We report the absorption of a diffusive spin current in a bulk-carrier compensated topological insulator: $Sn_{0.02}$-$Bi_{1.08}Sb_{0.9}Te_2S$ (Sn-BSTS). By injecting spins into a Sn-BSTS crystal from a ferromagnetic metal using spin pumping, we found that the magnetic damping of the ferromagnetic layer is enhanced due to the absorption of the spin current in the surface and bulk states of the topological insulator. We found that the damping enhancement depends critically on temperature, which allows us to disentangle the spin absorption in the surface and bulk states, owing to the nearly perfect carrier compensation in the bulk part at low temperature. Our results show that the absorption of the spin current is dominated by the surface state of the Sn-BSTS crystal at low temperature, whereas the spin absorption in the surface state is comparable to that in the bulk state near room temperature. The coexistence of the spin absorption in the surface and bulk states has been demonstrated in two different systems, where the surface state is coupled with the dynamical magnetization through the diffusive spin current or exchange coupling. These results will be essential for quantitative understanding of the spin absorption and spin-charge conversion due to the spin-momentum locked surface state of topological insulators.

PACS numbers: 72.25.Pn,72.25.Mk,75.76.+j

A topological insulator (TI) is a bulk electrical insulator with a two-dimensional metallic surface where the spin and momentum channels are locked to each other.[1–3] In a prototypical three-dimensional TI, Bi_2Se_3, a large spin-orbit interaction leads to a band inversion in the bulk and the formation of the topologically protected surface state. The spin-momentum locked surface state has been studied by transport measurements, as well as the angle-resolved photo-emission spectroscopy.[4–7] A recent transport experiment has shown that a charge current flowing in a Bi_2Se_3 film can exert a strong spin-orbit torque on an adjacent ferromagnetic metal, with a direction consistent with that expected from the topological surface state.[8] The spin-orbit torque originating from the TI is characterized by the charge-to-spin conversion efficiency, which is an order of magnitude larger than that of heavy metals at room temperature. The efficient generation of the spin-orbit torque makes this class of materials appealing for spintronic applications.[9–12]

The spin-momentum locked surface state of the prototypical TI has also been used for spin-to-charge conversion, the inverse process of the spin-torque generation. The spin-to-charge conversion has been quantified using spin pumping in ferromagnetic-metal/TI heterostructures.[13–17] In the heterostructures, injection of spins into the TI by the spin pumping leads to the generation of an electric voltage in the plane of the film. The spin transport measurements, including the spin-torque generation and spin pumping, however, have met with limited success due to the fact that the experiments have typically been conducted in the prototypical, but non-ideal, TI in which the surface states coexist with the bulk conduction. Because of the large bulk conductivity, the spin transport in the bulk part cannot be neglected in the TI, which makes it difficult to discuss the spin-transport properties in the surface and bulk states in TIs, separately.

For understanding the spin transport in TIs, quantifying the absorption of spins in the spin-momentum locked surface state is of particular importance. In the spin pumping, because of the short spin lifetime in the surface state due to the locking between the spin and momentum, sizable spins injected into a TI are absorbed in the surface state before diffusing into the bulk. In this paper, we report the absorption of a diffusive spin current in the surface and bulk states of a bulk-carrier compensated TI, $Sn_{0.02}$-$Bi_{1.08}Sb_{0.9}Te_2S$ (Sn-BSTS). Sn-BSTS displays a surface state Dirac point energy fully isolated from the bulk conduction, which results in very-low bulk carrier concentrations and strong domination of the conductance by surface currents below $T < 100$ K.[18] This property allows us

to quantify the absorption of a spin current in the surface states of the bulk crystal TI. To quantify the spin absorption in the surface state, we measured the spin pumping in a ferromagnetic-metal/paramagnetic-metal/Sn-BSTS heterostructure, where a diffusive spin current generated by the spin pumping is injected into the Sn-BSTS crystal through the paramagnetic metal with weak spin-orbit coupling.[19–22] By measuring ferromagnetic resonance (FMR) for the heterostructure, we found enhancement of the magnetic damping in the ferromagnetic film due to the absorption of the diffusive spin current in the surface and bulk states of the Sn-BSTS crystal. The enhanced magnetic damping of the ferromagnetic layer changes drastically by decreasing temperature, which is attributed to the suppression of the spin absorption in the bulk state. The strong suppression of the bulk contribution allows us to quantify the spin absorption purely in the surface state of the TI. A qualitatively similar trend in the temperature dependence of the damping enhancement has also been found in a system where a ferromagnetic layer is in direct contact with a Sn-BSTS crystal. These results illustrate an important role of the spin-momentum locked surface state of the TI crystal in the spin absorption, where the surface state is coupled with the dynamical magnetization through the diffusive spin current or exchange coupling.

Single crystals of the highly bulk insulating TI, Sn-BSTS, were grown by the vertical Bridgman technique as described in Ref 23. Figure 1(a) shows temperature T dependence of the in-plane electric resistivity $\rho_{\rm in}$ measured for the Sn-BSTS crystals with different thicknesses t. Here, $\rho_{\rm in} = (tw/l)R$, where w is the width of the crystals, l is distance between the voltage contacts, and R is the measured resistance. Figure 1(a) shows that for all the samples, $\rho_{\rm in}$ increases exponentially with decreasing T, attains maximum values around 150 K, and starts decreasing with decreasing T. This decrease shows the resistivity of the insulating bulk material has been short-circuited at low temperatures by the metallic surface state.[18] While the curves almost overlap at high temperatures, the ρ-value at low temperatures decreases significantly when reducing the thickness of the Sn-BSTS. This result demonstrates that the ratio between the surface and bulk contribution changes with thickness; the metallic surface states dominate the charge transport at low temperatures in the TI crystals.

The sample used for the spin pumping is a $Ni_{81}Fe_{19}$(Py) (20 nm)/Cu(10 nm)/Sn-BSTS heterostructure, capped with a 7-nm-thick SiO_2 film, where the numbers in parentheses represent the thickness (see Fig. 1(b)). The Py, Cu, and SiO_2 films were deposited on the Sn-BSTS crystal by rf magnetron sputtering at room temperature. Before the deposition,

the base pressure in the chamber was better than 3×10^{-6} Pa and the deposition pressure was 0.2 Pa. The thickness of the Sn-BSTS layers is around 300 μm, which is much thicker than the spin diffusion length of the bulk state of TIs. The thickness of the Cu layer, inserted between the Py and Sn-BSTS layers, is much thinner than the spin diffusion length of Cu, ~ 500 nm,[24] allowing us to neglect the relaxation of the diffusive spin current generated by the spin pumping in the Cu layer. For the measurements, the heterostructure was placed at the center of a coplanar waveguide as shown in Fig. 1(c). The signal line of the waveguide is 500 μm wide and the gaps between the signal line and the ground lines are designed to match to the characteristic impedance of 50 Ω. An in-plane external magnetic field $\mathbf{H}$ was applied along the signal line of the waveguide. Using a network analyzer and a microwave amplifier, we measured ferromagnetic resonance (FMR) for the Py/Cu/Sn-BSTS heterostructure at various temperatures T.

Figure 2 (a) shows magnetic field H dependence of microwave transmittance $|S_{21}|^2$ for the Py/Cu/Sn-BSTS heterostructure at the microwave frequency of $f = 6.0$ GHz and power of 1 W. As shown in Fig. 2(a), the microwave absorption due to the FMR appears around ± 65 mT. The FMR was measured at various microwave excitation frequencies f for the Py/Cu/Sn-BSTS heterostructure to determine the magnetic damping constant α from the FMR spectral width. Figure 2(b) shows the f dependence of the half-width half maximum ΔH of the FMR spectra at $T = 60$ K. Figure 2(b) shows that ΔH is well reproduced by the sum of the linewidth due to the magnetic damping α and the linewidth $\Delta H_{\rm ext}$ due to inhomogeneity: $\mu_0 \Delta H = (2\pi\alpha/\gamma) f + \mu_0 \Delta H_{\rm ext}$, where γ is the gyromagnetic ratio. The linear relationship between ΔH and f indicates that the linewidth broadening due to inhomogeneity of the microwave field can be neglected because this contribution depends on the excitation frequency; the additional linewidth due to the inhomogeneity of the microwave increases nonlinearly with decreasing the excitation frequency.[25,26] Therefore, the damping constant α of the Py/Cu/Sn-BSTS heterostructure can be determined from the slope of the linear fit to the experimental data shown in Fig. 2(b). The obtained values of the damping constant α for the Py/Cu/Sn-BSTS heterostructure are plotted as a function of temperature T in Fig. 3(a). For comparison, the temperature dependence of the damping constant α measured for a 20-nm-thick Py film, capped with 7-nm-thick SiO_2 film, is also shown in Fig. 3(a).

Figure 3(a) demonstrates that the magnetic damping α of the Py layer is enhanced by

attaching the Cu/Sn-BSTS film at all the temperatures studied. The enhancement of α can be attributed to the absorption of the diffusive spin current generated by the spin pumping in the surface and bulk states of the Sn-BSTS layer. In the Py/Cu/Sn-BSTS heterostructure, the spin pumping emits a spin-current from the Py layer into the Cu/Sn-BSTS layer. Since the thickness of the Cu layer is much thinner than the spin diffusion length of Cu, the relaxation of the generated spin current traveling in the Cu layer is negligible in the heterostructure. Thus, most of the spin current generated by the spin pumping diffuses into the Sn-BSTS layer, and the spin current is absorbed in the surface and bulk states of the Sn-BSTS layer. The spin absorption results in the enhanced angular momentum dissipation, or enhanced magnetic damping α, since the spin-current emission from the Py layer deprives the magnetization of the angular momentum.[27] This mechanism of the damping enhancement induced by the spin pumping indicates that the additional damping $\Delta\alpha = \alpha_{\mathrm{F/N/TI}} - \alpha_{\mathrm{F}}$ shown in Fig. 3(b) characterizes to the amount of spin angular momentum absorbed in the Sn-BSTS layer, where $\alpha_{\mathrm{F/N/TI}}$ and α_{F} are the magnetic damping constant for the Py/Cu/Sn-BSTS and Py films, respectively.

As shown in Figs. 1(a) and 3(b), both additional damping $\Delta\alpha$ and the resistivity ρ_{in} of the Sn-BSTS crystal change drastically around $T = 200$ K. This result allows us to quantify the spin absorption in the bulk and surface states. The temperature dependence of the additional magnetic damping $\Delta\alpha$ for the Py/Cu/Sn-BSTS in Fig. 3(b) allows to extract the absorption of the diffusive spin current in the surface state of the Sn-BSTS film, free from the ferromagnetic proximity effect. The spin absorption in the surface state of the Sn-BSTS film can be quantified from the damping enhancement at low temperature. At $T < 100$ K, thanks to the nearly perfect carrier compensation in the bulk part, the diffusive spin current generated by the spin pumping cannot diffuses into the bulk of the Sn-BSTS layer. This indicates that only the surface state of the Sn-BSTS film can be the absorber of the diffusive spin current generated by the spin pumping below 100 K. Figure 3(b) shows that at $T < 100$ K, the additional damping is $\Delta\alpha \sim 0.02$, which characterizes the absorption of the diffusive spin current in the surface state of the Sn-BSTS film.

The spin diffusion and absorption in the bulk of the Sn-BSTS film cannot be neglected at $T > 100$ K, since a sizable amount of bulk carriers are induced by increasing the temperature. The appearance of the bulk spin absorption leads to the increase of the additional damping with T as shown in Fig. 3(b); at $T > 100$ K, both the surface and bulk states contribute

to the damping enhancement, or the absorption of the diffusive spin current. Figure 3(b) demonstrates that the damping enhancement in the bulk state increases with T, and the spin absorption in the bulk part becomes comparable to that in the surface part at $T>$ 200 K. This is consistent with the carrier conduction of the surface and bulk states; the conduction is dominated by the bulk part at $T>$ 200 K [see Fig. 1(a)]. A qualitatively similar result was observed for a Py (20 nm)/Sn-BSTS film, capped with a SiO_2 (7 nm) film, as shown in Figs. 3(b) and 3(c). In the Py (20 nm)/Sn-BSTS heterostructure, the damping enhancement due to the spin pumping $\Delta\alpha$ changes drastically around $T = 150$ K. This result shows that the absorption of the spin current in the bulk part cannot be neglected near room temperature regardless of the mechanism of the coupling between the dynamical magnetization in the ferromagnetic layer and the surface state in the TI layer; because of the direct contact between the Py and Sn-BSTS layers in the Py (20 nm)/Sn-BSTS film, the surface states of the Sn-BSTS layer exchange-couples to the dynamical magnetization in the Py layer, which is different from the indirect coupling between the surface states and the dynamical magnetization through the diffusive spin current in the Py/Cu/Sn-BSTS film. Here, the direct deposition of a ferromagnet on a topological insulator can affect the topological surface state, potentially leading to a gap opening by the onset of an out-of-plane ferromagnetic order. The gap opening will affect the spin pumping especially when the Fermi level is within the band gap. However, previous studies show that the topologically protected surface states maintain their linear dispersion with a formation of a ferromagnet with in-plane magnetization.[28,29] Our observation of the efficient spin absorption in the surface state in the Py/Sn-BSTS heterostructure indicates that the possible change of the surface state due to the direct Py deposition plays a minor role in the present study due to the fact that the Py layer is in-plane magnetized and the Fermi level is far from the Dirac point.

Figure 3(b) shows that the additional damping at low temperature is comparable in the Py/Cu/Sn-BSTS and Py/Sn-BSTS heterostructures. This result indicates that the damping enhancement due to the surface state is comparable in magnitude despite the different spin-injection mechanisms; the surface state is coupled with the dynamical magnetization through the diffusive spin current or exchange coupling. In contrast to the surface spin absorption, the additional damping of the Py/Sn-BSTS heterostructure is clearly smaller than that of the Py/Cu/Sn-BSTS heterostructure above 200 K, where the bulk contribution appears, showing that the bulk spin absorption strongly depends on the device structure. This result

indicates ineffective spin pumping into the bulk of the Sn-BSTS crystal when the TI is in direct contact with the ferromagnetic metal, where the surface states exchange-couples to the dynamical magnetization.

To quantitatively discuss the spin absorption in the surface state of the Sn-BSTS film, we use the spin pumping model in the presence of the spin-orbit coupling, which takes into account the spin memory loss and spin accumulation at the interface.[30] In this model, when **H** is applied the in plane of a ferromagnetic/paramagnetic heterostructure, the additional magnetic damping $\Delta\alpha$ is expressed as[30]

$$\Delta\alpha = \frac{g\mu_{\mathrm{B}}\Gamma_0}{\mu_0 M_{\mathrm{s}} d}\left(\frac{1+6\eta\xi}{1+\xi}+\frac{\eta}{2(2+\xi)^2}\right), \tag{1}$$

where ξ is the backflow factor, which ranges between zero and infinity; $\xi = 0$ refers to the case where there is no backflow; $\xi = \infty$ indicates that the entire spin current pumped into the bulk flows back across the interface. Here, d is the thickness of the ferromagnetic layer, g is the g factor, μ_{B} is the Bohr magneton, M_{s} is the saturation magnetization, and Γ_0 is the mixing conductance across the interface. η is the parameter that characterizes the interface spin-orbit coupling effect. At $T < 100$ K, ξ is taken to be ∞ because of the absence of the bulk spin absorption. Thus, at low temperatures, Eq. (1) can be simplified as

$$\Delta\alpha = \frac{6g\mu_{\mathrm{B}}\Gamma_0\eta}{\mu_0 M_s d}. \tag{2}$$

In contrast to the absence of the bulk spin absorption at low temperatures, the bulk of the Sn-BSTS crystal is a spin sink around room temperature because the thickness of the TI layer, ~ 300 μm, is much larger than the spin diffusion length. This shows that, around room temperature, Eq. (1) can be simplified using $\xi = 0$. Using $\Delta\alpha \sim 0.02$ at $T < 100$ K and $\Delta\alpha \sim 0.04$ around room temperature with the above approximation and neglecting the temperature dependence of Γ_0, we obtain $\eta \sim 0.09$ for the Py/Cu/Sn-BSTS heterostructure. This is a reasonable value given that the Fermi vector is of the order of an inverse angstrom,[30] suggesting that further quantification of η in different systems will provide a way to characterize the interface spin-orbit coupling effect in a wide range of materials.

In summary, we have studied the absorption of a diffusive spin current in a bulk-carrier compensated TI: Sn-BSTS. We measured temperature dependence of the spin pumping for two different systems, Py/Cu/Sn-BSTS and Py/Sn-BSTS films, where the surface state is coupled with the dynamical magnetization through the diffusive spin current or exchange

coupling. We found that the damping enhancement due to the spin absorption depends critically on the temperature in both systems. This result allows to disentangle the spin absorption in the surface and bulk states of the Sn-BSTS crystal, thanks to the nearly perfect carrier compensation in the bulk part at low temperature. Our results show that the absorption of the spin current is dominated by the surface state of the TI at low temperature, whereas the spin absorption in the surface state is comparable to that in the bulk state near room temperature. These results will be essential for quantitative understanding of the spin absorption and spin-charge conversion due to the spin-momentum locked surface state of TIs.

The authors thank Kai Chen and Shufeng Zhang of University of Arizona for helpful discussions. This work was supported by PRESTO-JST (13415036, JPMJPR1323), JST-CREST (JPMJCR16F2), JSPS KAKENHI Grant Numbers 26220604, 26103004, 16H03847, JSPS Core-to-Core Program, and Spintronics Research Network of Japan (Spin-RNJ).

---

* ando@appi.keio.ac.jp

[1] M. Campisi, P. Hänggi, and P. Talkner, Rev. Mod. Phys. **83**, 1653 (2011).

[2] M. Z. Hasan and C. L. Kane, Rev. Mod. Phys. **82**, 3045 (2010).

[3] Y. Ando, J. Phys. Soc. Jpn. **82**, 102001 (2013).

[4] D. Hsieh, Y. Xia, D. Qian, L. Wray, J. Dil, F. Meier, J. Osterwalder, L. Patthey, J. Checkelsky, N. Ong, *et al.*, Nature **460**, 1101 (2009).

[5] D. Hsieh, Y. Xia, D. Qian, L. Wray, F. Meier, J. Dil, J. Osterwalder, L. Patthey, A. Fedorov, H. Lin, *et al.*, Phys. Rev. Lett. **103**, 146401 (2009).

[6] Y. Chen, J. Analytis, J.-H. Chu, Z. Liu, S.-K. Mo, X.-L. Qi, H. Zhang, D. Lu, X. Dai, Z. Fang, *et al.*, Science **325**, 178 (2009).

[7] Y. L. Chen, J.-H. Chu, J. G. Analytis, Z. K. Liu, K. Igarashi, H.-H. Kuo, X. L. Qi, S. K. Mo, R. G. Moore, D. H. Lu, M. Hashimoto, T. Sasagawa, S. C. Zhang, I. R. Fisher, Z. Hussain, and Z. X. Shen, Science **329**, 659 (2010).

[8] A. R. Mellnik, J. S. Lee, A. Richardella, J. L. Grab, P. J. Mintun, M. H. Fischer, A. Vaezi, A. Manchon, E.-A. Kim, N. Samarth, and D. C. Ralph, Nature **511**, 449 (2014).

[9] Y. Fan, P. Upadhyaya, X. Kou, M. Lang, S. Takei, Z. Wang, J. Tang, L. He, L.-T. Chang,

M. Montazeri, G. Yu, W. Jiang, T. Nie, R. N. Schwartz, Y. Tserkovnyak, and K. L. Wang, Nat. Mater. **13**, 699 (2014).

[10] K. Kondou, R. Yoshimi, A. Tsukazaki, Y. Fukuma, J. Matsuno, K. S. Takahashi, M. Kawasaki, Y. Tokura, and Y. Otani, Nat. Phys. **12**, 1027 (2016).

[11] Y. Wang, P. Deorani, K. Banerjee, N. Koirala, M. Brahlek, S. Oh, and H. Yang, Phys. Rev. Lett. **114**, 257202 (2015).

[12] J. Han, A. Richardella, S. A. Siddiqui, J. Finley, N. Samarth, and L. Liu, Phys. Rev. Lett. **119**, 077702 (2017).

[13] H. Wang, J. Kally, J. S. Lee, T. Liu, H. Chang, D. R. Hickey, K. A. Mkhoyan, M. Wu, A. Richardella, and N. Samarth, Phys. Rev. Lett. **117**, 076601 (2016).

[14] P. Deorani, J. Son, K. Banerjee, N. Koirala, M. Brahlek, S. Oh, and H. Yang, Phys. Rev. B **90**, 094403 (2014).

[15] M. Jamali, J. S. Lee, J. S. Jeong, F. Mahfouzi, Y. Lv, Z. Zhao, B. K. Nikolić, K. A. Mkhoyan, N. Samarth, and J.-P. Wang, Nano Lett. **15**, 7126 (2015).

[16] Y. Shiomi, K. Nomura, Y. Kajiwara, K. Eto, M. Novak, K. Segawa, Y. Ando, and E. Saitoh, Phys. Rev. Lett. **113**, 196601 (2014).

[17] K. Yamamoto, Y. Shiomi, K. Segawa, Y. Ando, and E. Saitoh, Phys. Rev. B **94**, 024404 (2016).

[18] S. Kushwaha, I. Pletikosić, T. Liang, A. Gyenis, S. Lapidus, Y. Tian, H. Zhao, K. Burch, J. Lin, W. Wang, *et al.*, Nat. Commun. **7**, 11456 (2016).

[19] S. Mizukami, Y. Ando, and T. Miyazaki, Phys. Rev. B **66**, 104413 (2002).

[20] Y. Tserkovnyak, A. Brataas, and G. E. W. Bauer, Phys. Rev. Lett. **88**, 117601 (2002).

[21] A. Brataas, Y. Tserkovnyak, G. E. W. Bauer, and B. I. Halperin, Phys. Rev. B **66**, 060404(R) (2002).

[22] A. Baker, A. Figueroa, L. Collins-McIntyre, G. Van Der Laan, and T. Hesjedal, Sci. Rep. **5** (2015).

[23] T. Misawa, Y. Fukuyama, Y. Okazaki, S. Nakamura, N. Nasaka, T. Sasagawa, and N. H. Kaneko, IEEE Trans. Instrum. Meas. **66**, 1489 (2017).

[24] H. Wang, C. Du, Y. Pu, R. Adur, P. C. Hammel, and F. Yang, Phys. Rev. Lett. **112**, 197201 (2014).

[25] G. Counil, J.-V. Kim, T. Devolder, C. Chappert, K. Shigeto, and Y. Otani, J. Appl. Phys. **95**, 5646 (2004).

[26] H. K. Lee, I. Barsukov, A. G. Swartz, B. Kim, L. Yang, H. Y. Hwang, and I. N. Krivorotov, AIP Adv. **6**, 055212 (2016).

[27] Y. Tserkovnyak, A. Brataas, G. E. W. Bauer, and B. I. Halperin, Rev. Mod. Phys. **77**, 1375 (2005).

[28] M. R. Scholz, J. Sánchez-Barriga, D. Marchenko, A. Varykhalov, A. Volykhov, L. V. Yashina, and O. Rader, Phys. Rev. Lett. **108**, 256810 (2012).

[29] J. Honolka, A. A. Khajetoorians, V. Sessi, T. O. Wehling, S. Stepanow, J.-L. Mi, B. B. Iversen, T. Schlenk, J. Wiebe, N. B. Brookes, A. I. Lichtenstein, P. Hofmann, K. Kern, and R. Wiesendanger, Phys. Rev. Lett. **108**, 256811 (2012).

[30] K. Chen and S. Zhang, Phys. Rev. Lett. **114**, 126602 (2015).

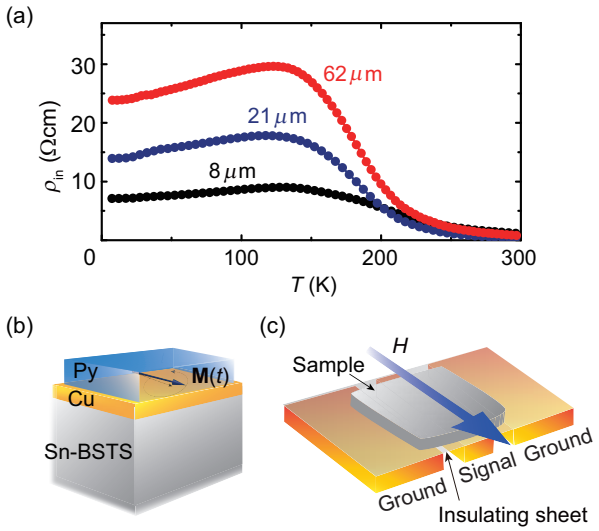

FIG. 1. (a) Temperature (T) dependence of the in-plane resistivity ($\rho_{\rm in}$) for the $Sn_{0.02}$-$Bi_{1.08}Sb_{0.9}Te_2S$ (Sn-BSTS) samples with different thicknesses t. The thickness t of the samples are 62 μm (red), 21 μm (blue), 8 μm (black). (b) A schematic illustration of the Py/Cu/Sn-BSTS heterostructure. The size of the Sn-BSTS crystal is 2 mm $\times$ 4 mm and that of the Py/Cu layer is 1 mm $\times$ 3 mm. (c) A schematic illustration of the experimental setup. The sample was placed on the coplanar waveguide for the microwave absorption measurement. The sample and waveguide are electrically disconnected by the insulating sheet.

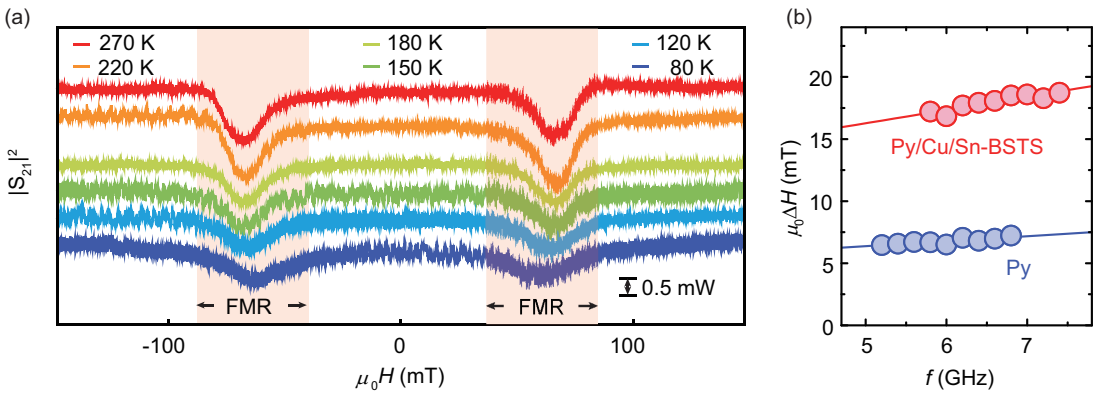

FIG. 2. (a) Magnetic field H dependence of microwave transmittance $|S_{21}|^2$ for the Py/Cu/Sn-BSTS layer at the microwave frequency of $f = 6.0$ GHz at various temperatures. The red colored areas represent FMR. (b) Microwave excitation frequency f dependence of the half-maximum half-width field ΔH at $T = 60$ K. The red solid circles are the experimental data for the Py/Cu/Sn-BSTS layer and the blue solid circles are the experimental data for the Py layer. The red and blue solid lines are the linear fit to the experimental data.

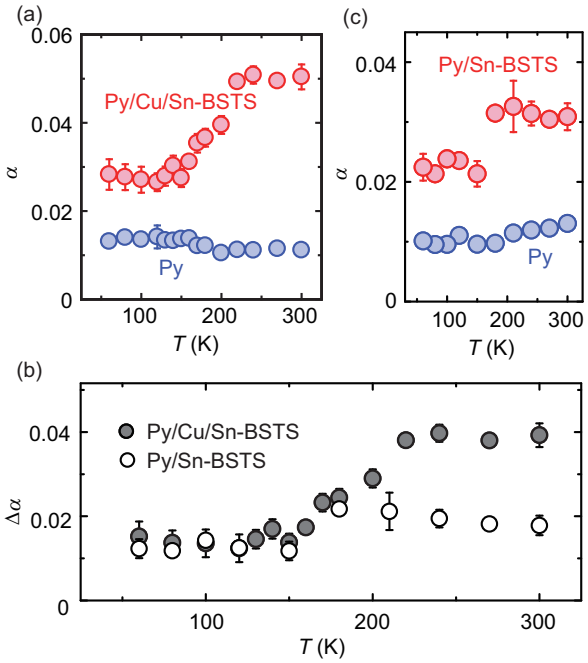

FIG. 3. (a) T dependence of the magnetic damping constant α for the Py/Cu/Sn-BSTS heterostructure (red solid circles) and the Py layer (blue solid circles). (b) T dependence of the additional damping constant $\Delta\alpha$ for the Py/Cu/Sn-BSTS and Py/Sn-BSTS heterostructures. The solid circles are the experimental data of the additional damping constant $\Delta\alpha = \alpha_{\mathrm{F/N/TI}} - \alpha_{\mathrm{F}}$, where $\alpha_{\mathrm{F/N/TI}}$ and α_{F} are the magnetic damping constant for the Py/Cu/Sn-BSTS heterostructure and the Py film, respectively. The open circles are the experimental data of the additional damping constant $\Delta\alpha = \alpha_{\mathrm{F/TI}} - \alpha_{\mathrm{F}}$, where $\alpha_{\mathrm{F/TI}}$ is the magnetic damping constant for the Py/Sn-BSTS heterostructure. (c) T dependence of the magnetic damping constant α for the Py/Sn-BSTS heterostructure (red solid circles) and the Py layer (blue solid circles).